

# Collisional-Radiative Model for Spectroscopic Diagnostic of Optically Thick Helium Plasma

Keiji SAWADA, Yusuke YAMADA, Takamasa MIYACHIKA, Naomichi EZUMI<sup>1)</sup>,  
Atsushi IWAMAE<sup>2)</sup> and Motoshi GOTO<sup>3)</sup>

*Faculty of Engineering, Shinshu University, 4-17-1 Wakasato, Nagano 380-8553, Japan*

<sup>1)</sup>*Nagano National College of Technology, 716 Tokuma, Nagano 381-8550, Japan*

<sup>2)</sup>*Japan Atomic Energy Agency, 801-1 Mukoyama, Naka, Ibaraki 311-0193, Japan*

<sup>3)</sup>*National Institute for Fusion Science, 322-6 Oroshi-cho, Toki 509-5292, Japan*

(Received 7 September 2009 / Accepted 1 November 2009)

We have included the effect of radiation trapping in a collisional-radiative model of neutral helium atoms developed by Goto [M. Goto, *JQSRT* **76**, 331 (2003)], which is used to determine the electron temperature and density in plasmas from visible emission line intensities of atoms. In addition to the electron temperature and density, photo-excitation events from the ground state  $1^1S$  to the  $2^1P$ ,  $3^1P$ , and  $4^1P$  states per second per one atom are treated as fitting parameters to reproduce the population density obtained by spectroscopic measurement. The model has been applied to an RF plasma at Shinshu University, Japan. The electron temperature and density and the contribution of radiation trapping to the population density of excited states are evaluated.

© 2010 The Japan Society of Plasma Science and Nuclear Fusion Research

**Keywords:** radiation trapping, helium plasma, collisional-radiative model, electron density, electron temperature, metastable state, RF plasma

DOI: 10.1585/pfr.5.001

## 1. Introduction

Analysis of the intensity of atomic line radiation by the collisional-radiative model is a standard technique for determining the electron temperature and density in helium plasmas [1–3]. When using the diagnostic, generally, we have to evaluate the contribution of radiation trapping [4] to the population density of excited states. Because emission or absorption in one location depends on the radiation flux coming from the rest of the plasma, a self-consistent treatment of radiation trapping and population density is necessary. However, for convenience, in many cases the effect of radiation trapping is neglected or treated by the escape factor method [4], which assumes a spatial distribution of excited states without solving the equation of radiation trapping.

We have previously developed an iterative computational code for solving the radiative transfer equation coupled with the collisional-radiative rate equation [5]. In this study, we propose a simple method that can easily be applied to the spectroscopic diagnostic. We treat photo-excitation events from the ground state  $1^1S$  to the  $2^1P$ ,  $3^1P$ , and  $4^1P$  states per second per one atom as fitting parameters to reproduce the population density obtained by spectroscopic measurement. In this paper, the ionizing plasma [6] is considered. We extend a model developed by Goto [2] to include the effect of radiation trapping. Finally, we apply the code to an RF helium plasma at Shinshu University, Japan.

author's e-mail: ksawada@gipwc.shinshu-u.ac.jp

## 2. Model

According to the collisional-radiative model, if photo-excitation is neglected, the temporal variation of the population density of an excited state  $p$  can be described by rate equations for the ionizing plasmas, which are

$$\begin{aligned} dn(p)/dt = & \sum_{q < p} C(q, p)n_en(q) \\ & + \sum_{q > p} \{F(q, p)n_e + A(q, p)\}n(q) \\ & - \left\{ \left( \sum_{q < p} F(p, q) + \sum_{q > p} C(p, q) + S(p) \right) n_e \right. \\ & \left. + \sum_{q < p} A(p, q) \right\} n(p), \end{aligned} \quad (1)$$

where  $C(p, q)$  is the excitation rate coefficient for electron collisions from state  $p$  to  $q$ , and  $F(q, p)$  is the inverse de-excitation rate coefficient.  $A(p, q)$  is the spontaneous transition probability from  $p$  to  $q$ , and  $S(p)$  is the ionization rate coefficient for state  $p$ .

If photo-excitation from the ground state is included, Eq. (1) is extended as follows,

$$\begin{aligned} dn(p)/dt = & \sum_{q < p} C(q, p)n_en(q) \\ & + \sum_{q > p} \{F(q, p)n_e + A(q, p)\}n(q) \\ & - \left\{ \left( \sum_{q < p} F(p, q) + \sum_{q > p} C(p, q) + S(p) \right) n_e \right. \end{aligned}$$

$$\begin{aligned}
 & + \left. \sum_{q < p} A(p, q) \right\} n(p) \\
 & + \delta_{p,2^1P} I_{2^1P} n(1^1S) + \delta_{p,3^1P} I_{3^1P} n(1^1S) \\
 & + \delta_{p,4^1P} I_{4^1P} n(1^1S) + \dots, \quad (2)
 \end{aligned}$$

where  $\delta_{p,2^1P}$ ,  $\delta_{p,3^1P}$  and  $\delta_{p,4^1P}$  are functions of two states; their values are 1 if the states are equal, and 0 otherwise. The parameters  $I_{2^1P}$ ,  $I_{3^1P}$  and  $I_{4^1P}$  are the photo-excitation rates from the ground state  $1^1S$  to the  $2^1P$ ,  $3^1P$ , and  $4^1P$  states per one atom, respectively. Induced emission is neglected because we consider non-equilibrium ionizing plasmas [6]. Each  $L$  (the orbital angular momentum quantum number) level having principal quantum number  $n \leq 7$  is treated individually except for levels having  $L \geq 3$  [2]. These latter levels of the same  $n$  are bound together to form a single level, which is denoted as  $F$  in this paper.

According to the quasi-steady-state solution [6, 7], Eq. (1) is approximated to 0 for all the states except the ground state  $1^1S$  and the metastable states  $2^1S$  and  $2^3S$ :

$$\frac{d}{dt} n(p) = 0. \quad (3)$$

Thus, instead of the coupled differential equations, Eq. (2), we have a set of coupled linear equations, Eq. (3). In this paper, the contribution of photo-excitation from the  $1^1S$  to singlet  $P$  states higher than  $4^1P$  are neglected because emission lines whose upper states are higher than  $4^1P$  were not observed in our spectroscopic experiment (reported below).

Solving Eq. (3) yields the population density of an excited state  $p$  in the form

$$\begin{aligned}
 n(p) = & r_1(p)n(1^1S)n_e + r_2(p)n(2^1S)n_e \\
 & + r_3(p)n(2^3S)n_e + r_4(p)n(1^1S)I_{2^1P} \\
 & + r_5(p)n(1^1S)I_{3^1P} + r_6(p)n(1^1S)I_{4^1P}, \quad (4)
 \end{aligned}$$

where  $r_1(p)$ ,  $r_2(p)$ ,  $r_3(p)$ ,  $r_4(p)$ ,  $r_5(p)$ , and  $r_6(p)$  are the population coefficients, each of which is a function of  $n_e$  and  $T_e$ . The first three terms denote the traditional ionizing plasma component [6], while the last three are newly introduced. Using our model, we can determine the parameters of  $n_e$ ,  $T_e$ ,  $I_{2^1P}$ ,  $I_{3^1P}$ ,  $I_{4^1P}$ ,  $n(1^1S)$ ,  $n(2^1S)$ , and  $n(2^3S)$  experimentally.

The accuracy of the model depends on the reliability of the adopted cross section data for the electron impact transition; following Ref. [2], accurate cross sections calculated by the convergent close-coupling method [8–10] and the R-matrix with pseudostates method [11] are used in the present model. The rate coefficients for processes involving electron collisions are calculated by integrating the cross sections over a Maxwellian energy distribution.

### 3. Experimental

We applied the above model to an RF helium plasma at Shinshu University, Japan. Figure 1 shows a schematic view of the apparatus, consisting of a Pyrex glass tube

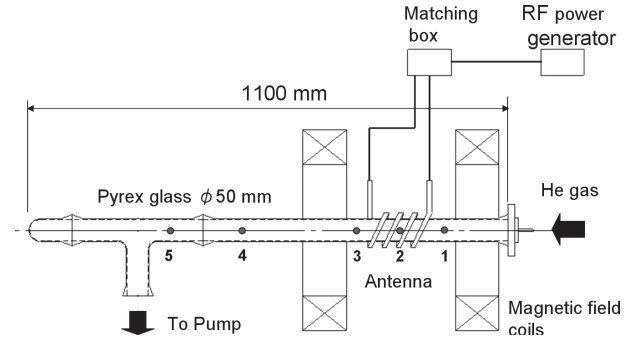


Fig. 1 Schematic view of the apparatus.

Table 1 Neutral helium emission lines observed in the experiment.

Transition	Wavelength [nm]	A coefficient [ $10^8 \text{ s}^{-1}$ ]
$4^3P - 2^3S$	318.77	0.0505
$3^3P - 2^3S$	388.87	0.09478
$4^1P - 2^1S$	396.47	0.0717
$5^3D - 2^3P$	402.62	0.117
$5^3S - 2^3P$	412.08	0.0430
$5^1D - 2^1P$	438.79	0.0907
$5^1S - 2^1P$	443.76	0.0313
$4^3D - 2^3P$	447.15	0.251
$4^3S - 2^3P$	471.32	0.106
$4^1D - 2^1P$	492.19	0.202
$3^1P - 2^1S$	501.57	0.1338
$4^1S - 2^1P$	504.77	0.0655
$3^3D - 2^3P$	587.57	0.706
$3^1D - 2^1P$	667.82	0.638
$3^3S - 2^3P$	706.53	0.278
$3^1S - 2^1P$	728.14	0.181

50 mm in diameter and 1100 mm in length, and an RF antenna. An RF power generator connected to a matching box supplied 100 W of power at 13.56 MHz. A pair of solenoids around the source produced magnetic fields of about 0.012 T at position 2 in Fig. 1. A base pressure of  $1.2 \times 10^{-4}$  Pa was maintained using a diffusion-rotary pump system. Helium gas was fed through a mass flow controller, and the pressure was maintained at 4.0 Pa.

We measured the intensities of the neutral helium emission lines listed in Table 1 at positions 1–5 in Fig. 1. These emission lines are optically thin. The line-of-sight is scanned by shifting a collecting lens vertically at each position to apply the Abel inversion and obtain emission powers,  $A(p, q)n(p)h\nu$ , as a function of the plasma radius. The collected light was fed via an optical fiber to a Czerny-Turner spectrometer with a CCD camera (Hamamatsu C5095, M6296-01). The optical fiber with the collecting lens provides approximately 2 mm spatial resolution. The sensitivity of the optical system was abso-

lutely calibrated using a calibrated xenon lamp light source (Hamamatsu L7810).

## 4. Results and Discussion

Figures 2(a) and 2(b) show the line-of-sight integrated emission powers of the spectral lines of the singlet and triplet states obtained from signals of the absolutely calibrated optical system, respectively, at position 2 in Fig. 1. These data were Abel-inverted, and the emission powers of the spectral lines in Table 1 were calculated as a function of the plasma radius. Figures 3(a) and 3(b) show the results of Abel inversion.

The large increase in intensity at  $r = 0$  mm in Figs. 3(a) and 3(b) is characteristic of position 2 which is located in the RF antenna. As an example of the other positions, Figs. 4(a) and 4(b) show the line-of-sight inte-

grated emission powers of the spectral lines at position 4, and Figs. 5(a) and 5(b) show the results of Abel inversion.

Figure 6 shows the population distribution of the singlet and triplet states at position 2 ( $r = 0$  mm) in Fig. 1.

The parameters  $n_e$ ,  $T_e$ ,  $I_{2^1P}$ ,  $I_{3^1P}$ ,  $I_{4^1P}$ ,  $n(2^1S)$ , and  $n(2^3S)$  on the right-hand side of Eq. (4) were determined by least squares, i.e., by minimizing the next function,

$$f(n_e, T_e, I_{2^1P}, I_{3^1P}, I_{4^1P}, n(2^1S), n(2^3S)) \equiv \sum_p \left( \frac{n(p) - n_{\text{exp}}(p)}{n_{\text{exp}}(p)} \right)^2, \quad (5)$$

where  $n(p)$  is the left-hand side of Eq. (4), and  $n_{\text{exp}}(p)$  denotes the population density determined by spectroscopic measurement. The summation was performed for the upper states of all the transitions in Table 1. In this study, the density of the ground state atom,  $9.7 \times 10^{20} \text{ m}^{-3}$ , which was

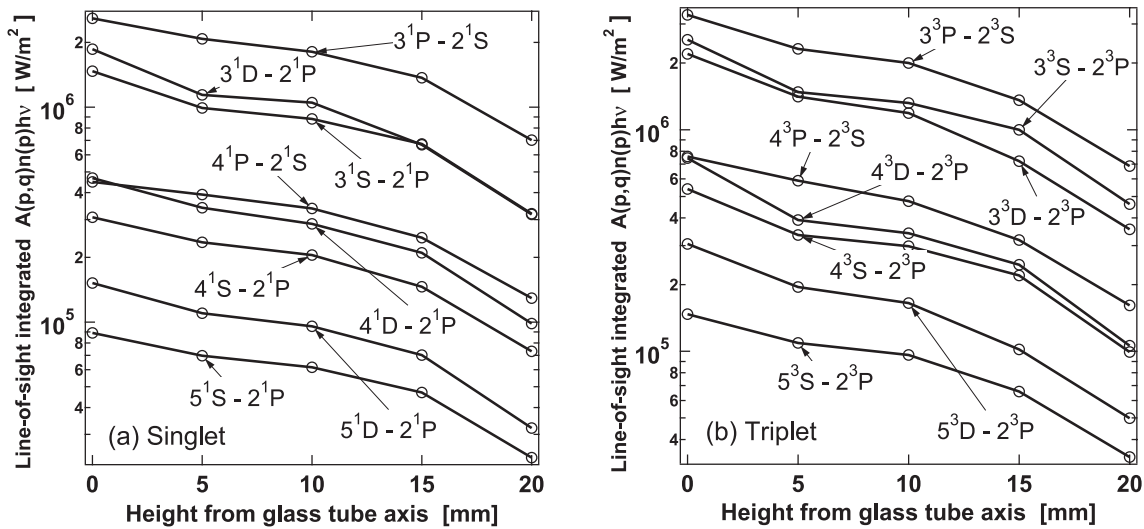


Fig. 2 Line-of-sight integrated  $A(p, q)n(p)hv$  at position 2 in Fig. 1. (a) Singlet and (b) Triplet states.

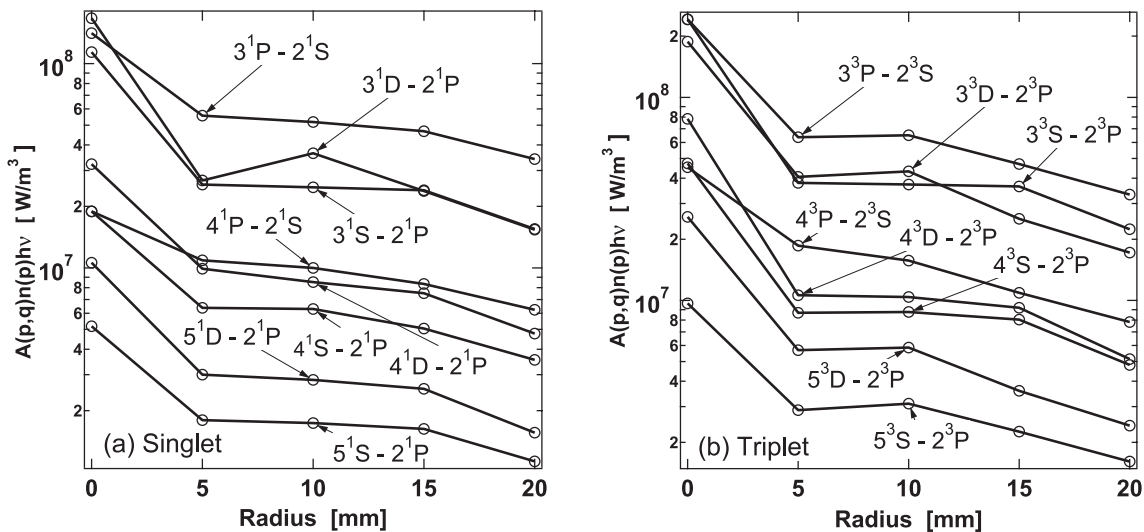


Fig. 3  $A(p, q)n(p)hv$  obtained by Abel inversion at position 2 in Fig. 1. (a) Singlet and (b) Triplet states.

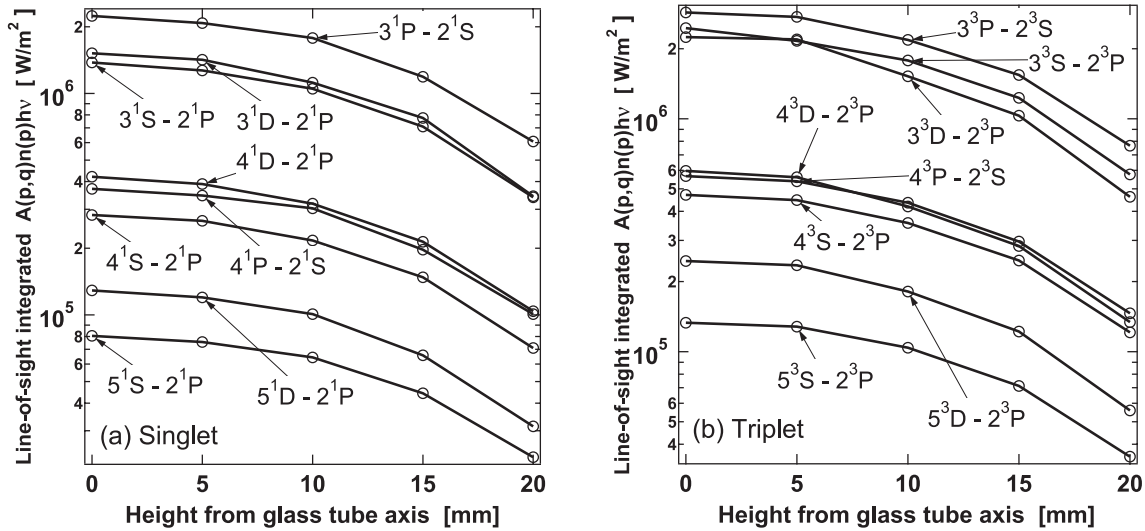


Fig. 4 Line-of-sight integrated  $A(p, q)n(p)hv$  at position 4 in Fig. 1. (a) Singlet and (b) Triplet states.

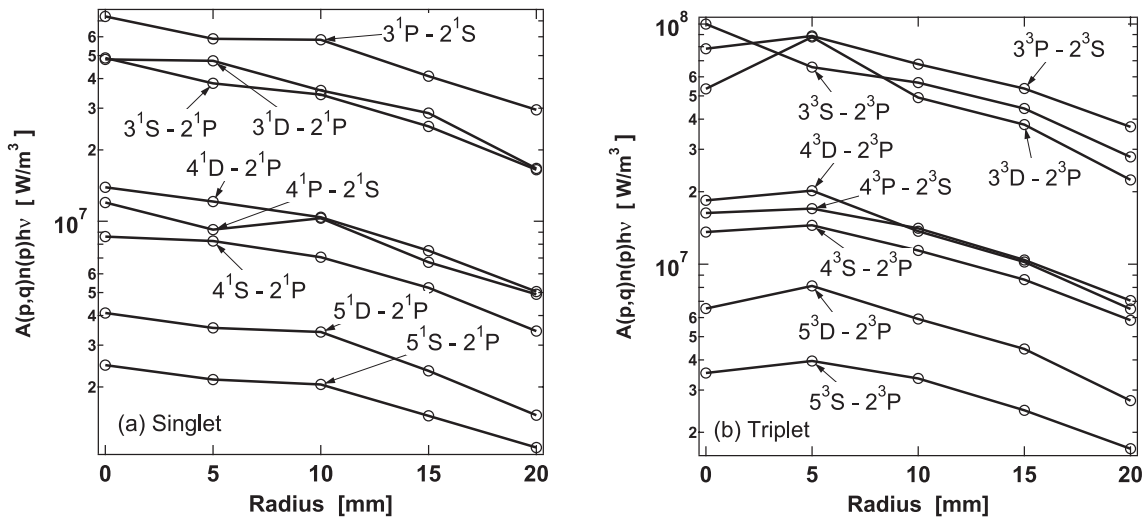


Fig. 5  $A(p, q)n(p)hv$  obtained by Abel inversion at position 4 in Fig. 1. (a) Singlet and (b) Triplet states.

evaluated from the gas pressure with the ideal-gas law, was used for  $n(1^1S)$ . By changing the values of each parameter, the best combination of parameter values was numerically determined.

The population density calculated with the optimized parameters is shown in Fig. 6. The experimentally obtained population was reproduced well by the least-squares fit. Most of the population of  $3^1P$  and  $4^1P$  is produced by photo-excitation from the ground state. The influence of photo-excitation to the  $3^1P$  and  $4^1P$  states on the population density of the other states is small because of the low electron density in the present experiment. Negligence of photo-excitation to the singlet  $P$  states higher than  $4^1P$  is thus justified. Similarly, the  $2^1P$  state produced by the photo-excitation decays into  $1^1S$  and  $2^1S$  by the radiative transition. The subsequent electron impact excitation from  $1^1S$  and  $2^1S$  is included in  $r_1(p)n(1^1S)n_e$

and  $r_2(p)n(2^1S)n_e$  in Eq. (4). Because the contribution of  $r_4(p)n(1^1S)I_{2^1P}$  to  $n \geq 3$  states, which originate from electron impact excitation from  $2^1P$ , is negligible in the present experiment, we cannot determine the accurate value of  $I_{2^1P}$  in the least-squares fit. Thus,  $r_4(p)n(1^1S)I_{2^1P}$  is omitted in Fig. 6.

For other states, the populations are produced mainly by the electron impact from the ground state, except for the singlet and triplet  $D$  states, where electron impact excitation from the singlet and triplet metastable states is significant.

Figures 7(a) and 7(b) show the electron temperature and density, determined using the proposed method, respectively. At position 2 ( $r = 0$  mm), which is in the RF antenna, the electron density has a high value. This is the origin of the intensity increase at  $r = 0$  mm in Fig. 3. At position 1, which is close to the end of the discharge tube,

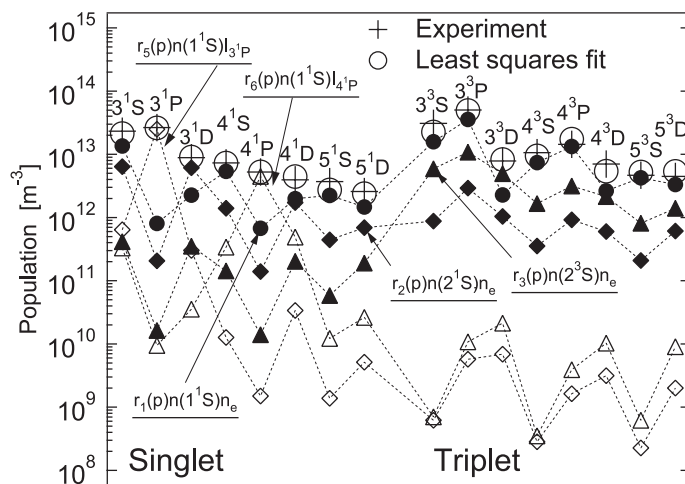


Fig. 6 Population distribution of singlet and triplet states at position 2 ( $r = 0$  mm) in Fig. 1. Pluses: spectroscopic measurement; open circles: result of the least-squares fit calculated using Eq. (4) with optimized parameters of  $n_e$ ,  $T_e$ ,  $I_{3^1P}$ ,  $I_{4^1P}$ ,  $n(2^1S)$ , and  $n(2^3S)$ . The contribution of each term of Eq. (4) is also shown. Closed circles:  $r_1(p)n(1^1S)n_e$ ; closed diamonds:  $r_2(p)n(2^1S)n_e$ ; closed triangles:  $r_3(p)n(2^3S)n_e$ ; open diamonds:  $r_5(p)n(1^1S)I_{3^1P}$ ; open triangles:  $r_6(p)n(1^1S)I_{4^1P}$ .

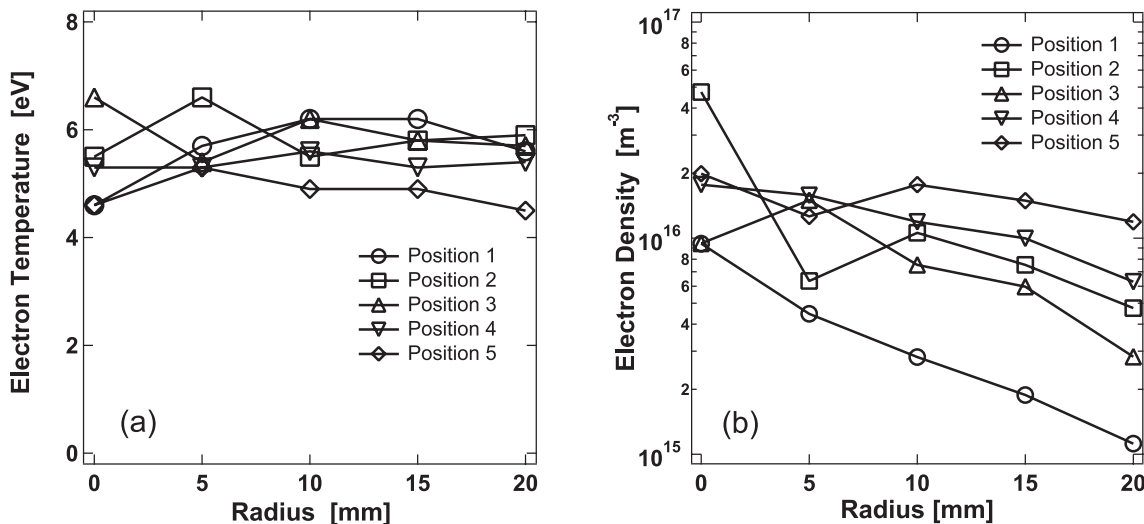


Fig. 7 Radial profiles of (a) electron temperature  $T_e$  and (b) electron density  $n_e$ .

the electron density is small. The electron temperature is roughly uniform in the plasma.

Figure 8 shows  $I_{3^1P}$  and  $I_{4^1P}$  at positions 2 and 4 in Fig. 1. At position 2 ( $r = 0$  mm),  $I_{3^1P}$  and  $I_{4^1P}$  are larger than that at position 4 ( $r = 0$  mm). The difference is attributed to the large population densities of the excited states  $n = 3$  and  $n = 4$  at position 2 ( $r = 0$  mm) due to the high electron density at that position; the radiation fields produced by emission from the upper states at position 2 are stronger than those at position 4.

Figure 9 shows  $n(2^1S)$  and  $n(2^3S)$  at positions 2 and 4. The figure indicates that the densities of the metastable states are roughly uniform in the plasma. The densities of the metastable states in Fig. 9 confirm that the quasi-steady-state approximation, Eq. (3), does not hold for the

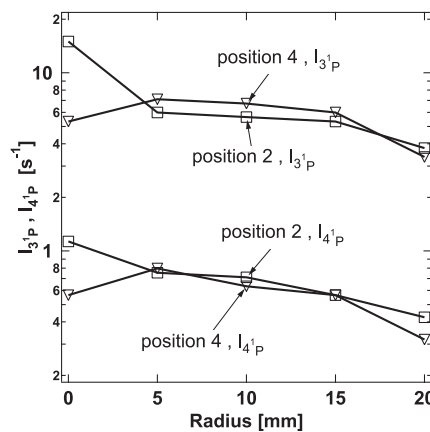


Fig. 8  $I_{3^1P}$ ,  $I_{4^1P}$  at positions 2 and 4 in Fig. 1.

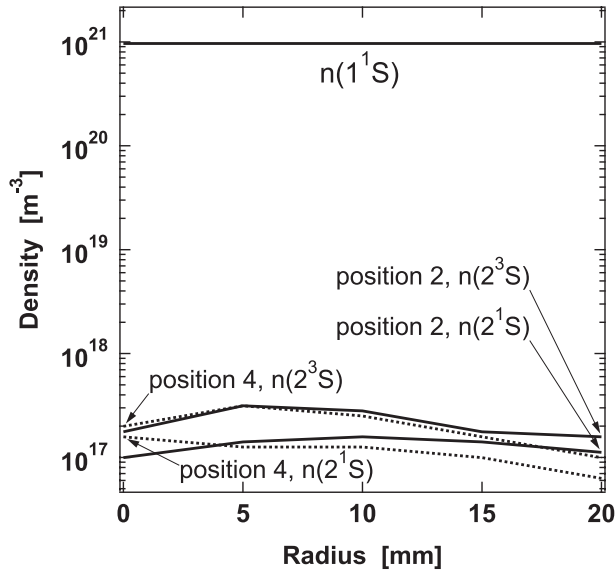


Fig. 9 Radial profiles of the population of metastable states  $n(2^1S)$  and  $n(2^3S)$ . The ground state density  $n(1^1S)$  is also shown.

Table 2 Mean free paths for photon absorption at the central frequency of the spectral lines.

Transition	$1/(\text{absorption coefficient})$ [m]
$1^1S - 2^1P$	$4.8 \times 10^{-5}$
$1^1S - 3^1P$	$2.0 \times 10^{-4}$
$1^1S - 4^1P$	$4.9 \times 10^{-4}$
$2^1S - 2^1P$	$9.6 \times 10^{-1}$
$2^1S - 3^1P$	$9.8 \times 10^0$
$2^1S - 4^1P$	$3.7 \times 10^1$
$2^3S - 2^3P$	$1.3 \times 10^0$
$2^3S - 3^3P$	$3.0 \times 10^1$
$2^3S - 4^3P$	$1.0 \times 10^2$

metastable states  $2^1S$  and  $2^3S$  in the present case.

We attempted to add the ground state atom density  $n(1^1S)$  to the parameters in Eq. (5). The result of the least-squares fit was almost the same as that shown in Fig. 6.

Table 2 gives the reciprocals of the absorption coefficients at the central frequency of the spectral lines, which correspond to the mean free paths for photon absorption at that frequency. In the calculation, thermal Doppler broadening at 300 K is assumed, and the densities of the ground state atom and the metastable atom in Fig. 9 are used. Table 2 indicates that photo-excitation from the singlet and triplet metastable states is small because the mean free paths are larger than the scale of the plasma.

Figure 10 shows the excitation and de-excitation flows at position 2 ( $r = 0$  mm). The largest inflow and outflow for each state and other significant flows are presented. Except for the singlet  $P$  states, the dominant inflow and out-

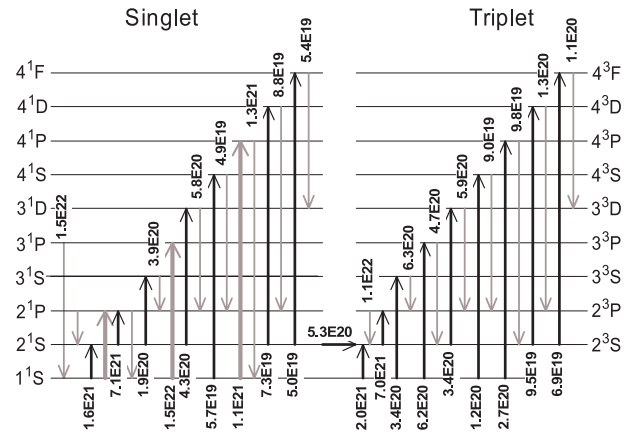


Fig. 10 Excitation and de-excitation flows at position 2 ( $r = 0$  mm). The largest inflow and outflow of each state and other significant flows are drawn. Black line, thin gray line, and thick gray line denote the transitions by electron collision, spontaneous emission, and photo-excitation, respectively. For example, 1.5E22 denotes  $1.5 \times 10^{22} \text{ m}^{-3} \text{ s}^{-1}$ .

flow of each state is caused by excitation from the ground state or the metastable states by electron impact and spontaneous emission to the lower states, respectively. Such a balance is characteristic of low electron density ionizing plasmas [6]. The dominant inflow for the singlet  $P$  states is caused by photo-excitation. As mentioned earlier, the amount of photo-excitation to the singlet  $2^1P$  state was not determined by our analysis, so we cannot estimate the emission flow from the  $2^1P$  state to the lower states  $1^1S$  and  $2^1S$ . However, because the populations of  $1^1S$  and  $2^1S$  are determined as shown in Fig. 9, we can calculate the excitation flows from  $1^1S$  and  $2^1S$ .

## 5. Conclusion

We have constructed a collisional-radiative model of neutral helium atoms that includes parameters of photo-excitation rate from a ground state atom to determine the electron temperature and density of plasmas in which the effect of radiation trapping cannot be neglected. The method reported in this paper has been applied to an RF plasma at Shinshu University. From the intensity of visible helium lines, the electron temperature and density and the densities of the singlet and triplet metastable state atoms are determined. The contribution of radiation trapping to the population density of the excited states is also estimated.

The proposed method has been applied to a low electron density plasma. However, it is also expected to be effective for higher electron density plasmas such as fusion plasmas, where the transition among excited states by electron impact cannot be neglected. We hope that this method will be tested for higher electron density plasmas and used as a standard diagnostic tool.

## Acknowledgements

This research was partially supported by Grants-in-Aid for Scientific Research (C), 15540470 and 21540508, from the Japan Society for the Promotion of Science, and by the NIFS Collaborative Research Program. The authors thank S. Koyama, N. Yamaguchi, K. Moteki, K. Takahashi, and R. Hattori for their experimental assistance and data analysis.

- [1] T. Fujimoto, *JQSRT* **21**, 439 (1978).
- [2] M. Goto, *JQSRT* **76**, 331 (2003).

- [3] M. Goto, S. Morita, K. Sawada, T. Fujimoto and S. Yamamoto, *Phys. Plasmas* **10**, 1402 (2003).
- [4] A.F. Molisch and B.P. Oehry, *Radiation Trapping in Atomic Vapours* (Oxford University Press, 1998).
- [5] K. Sawada, *J. Plasma Phys.* **72**, 1025 (2006).
- [6] T. Fujimoto, *Plasma Spectroscopy* (The International Series of Monographs on Physics, 123, Oxford University Press, 2004).
- [7] K. Sawada and T. Fujimoto, *Phys. Rev. E* **49**, 5565 (1994).
- [8] D.V. Fursa and I. Bray, *Phys. Rev. A* **52**, 1279 (1995)
- [9] I. Bray and D.V. Fursa, *J. Phys. B* **28**, L197 (1995).
- [10] D.V. Fursa and I. Bray, *J. Phys. B* **30**, 757 (1997).
- [11] K. Bartschat, *J. Phys. B* **31**, L469 (1998).